LA-UR-13-25416

Approved for public release; distribution is unlimited.

Title: MCNP6 Cerenkov Radiation Feature Verification

Author(s): Durkee, Joe W. Jr.
            James, Michael R.

Intended for: Report

Issued: 2013-07-17

Los Alamos
NATIONAL LABORATORY
——— EST. 1943 ———

MCNP6 Cerenkov Radiation Feature Verification

Joe W. Durkee, Jr. and Michael R. James
Los Alamos National Laboratory
jdurkee@lanl.gov
505-665-0530
Fax: 505-665-2897
PO Box 1663, MS C921
Los Alamos, NM 87545

ABSTRACT

The MCNP6 code has being upgraded to treat Cerenkov radiation emission. Emission is performed using the Frank-Tamm Cerenkov theory with piecewise-constant coefficients. This document discusses preliminary verification efforts for the Cerenkov feature. Tests were conducted using MCNP6 version MCNP6_Beta3_branch_r. The Frank-Tamm formulation has been coded in an auxiliary Perl script **cr.pl**. Comparisons of the photon production per wavelength bin and the aggregate photon production are made for 4-MeV electrons and 4000-MeV alphas in water using MCNP6 and **cr.pl**. The agreement is excellent. Verification calculations for the spectrum of light emerging from the surface of the water are presented for constant, Cauchy, and Sellmeier treatments of the refractive index. Efforts to conduct validation studies were limited by lack of time and limited useful measured data.

KEYWORDS: MCNP6; Cerenkov.

Contents

Figures

Acronyms

ENDF	Evaluated Nuclear Data File
LANL	Los Alamos National Laboratory
MCNP6	LANL Monte Carlo radiation transport code

1. INTRODUCTION

MCNP6 (Goorley et al., 2011) is a Monte Carlo particle (radiation quanta) radiation-transport code that is developed at Los Alamos National Laboratory (LANL). MCNP6 offers an assortment of features that provide detailed modeling and assessment capabilities. These features include three-dimensional (3-D) geometry modeling, continuous-energy transport, transport of 36 different types of fundamental particles as well as 2000+ types of heavy ions, delayed neutron and gamma radiation treatment, isotopic transmutation, the interaction of low- and high-energy radiation with matter, a variety of source and tally options, interactive graphics, and support for a variety of sequential and multiprocessing computer platforms. MCNP6 has a world-wide user base consisting of approximately 10000 researchers, designers, and analysts whose applications encompass accelerator design, nuclear reactor physics, isotopic transmutation, cancer diagnostics and therapy, geophysics, active and passive interrogation involving prompt and delayed radiation, and space applications.

MCNP6 has recently been updated to treat photon transport with energies down to 1eV. With this upgrade, Cerenkov photon generation is now being added.

In the following section, the theory of Cerenkov radiation is briefly reviewed. Formulations that are being implemented in MCNP6 are then developed. Section 3 presents verification efforts.

2. CERENKOV RADIATION

Cerenkov emission was discovered in 1934 (Cerenkov, 1934). Theoretical study of the phenomenon followed in 1937 (Frank and Tamm, 1937) using classical electrodynamics (Frank and Tamm, 1937) and later by Fermi (Fermi, 1940). We provide a brief review of the theory and the formulations implemented in MCNP6. For context purposes, the following section is included to illustrate where optical photons exist within the extent of the electromagnetic spectrum. Figure 1 contains images of Cerenkov, Frank, and Tamm.

Figure 1.   Cerenkov, Frank, and Tamm (nobelprize.org).

2.1.   Electromagnetic Spectrum

MCNP6 can treat photon transport down to 1 eV. Optical photons have energies on the order of a few eV, as illustrated in electromagnetic spectrum shown in Figures 2a and 2b.
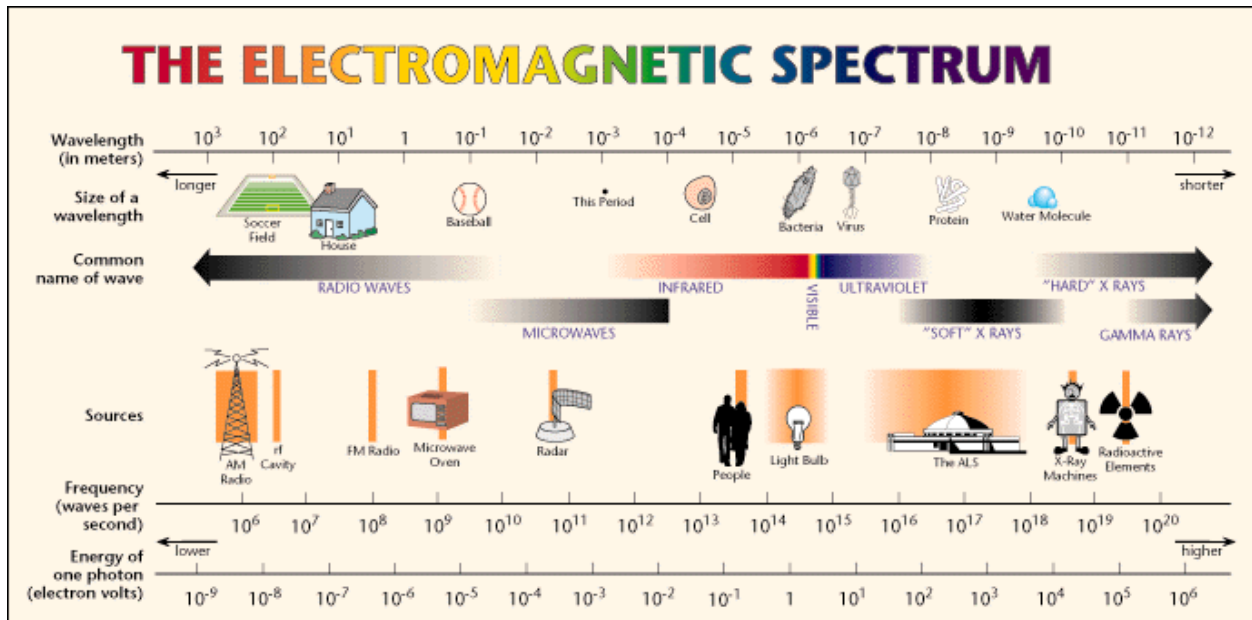
Figure 2a. Electromagnetic spectrum (www.lbl.gov).
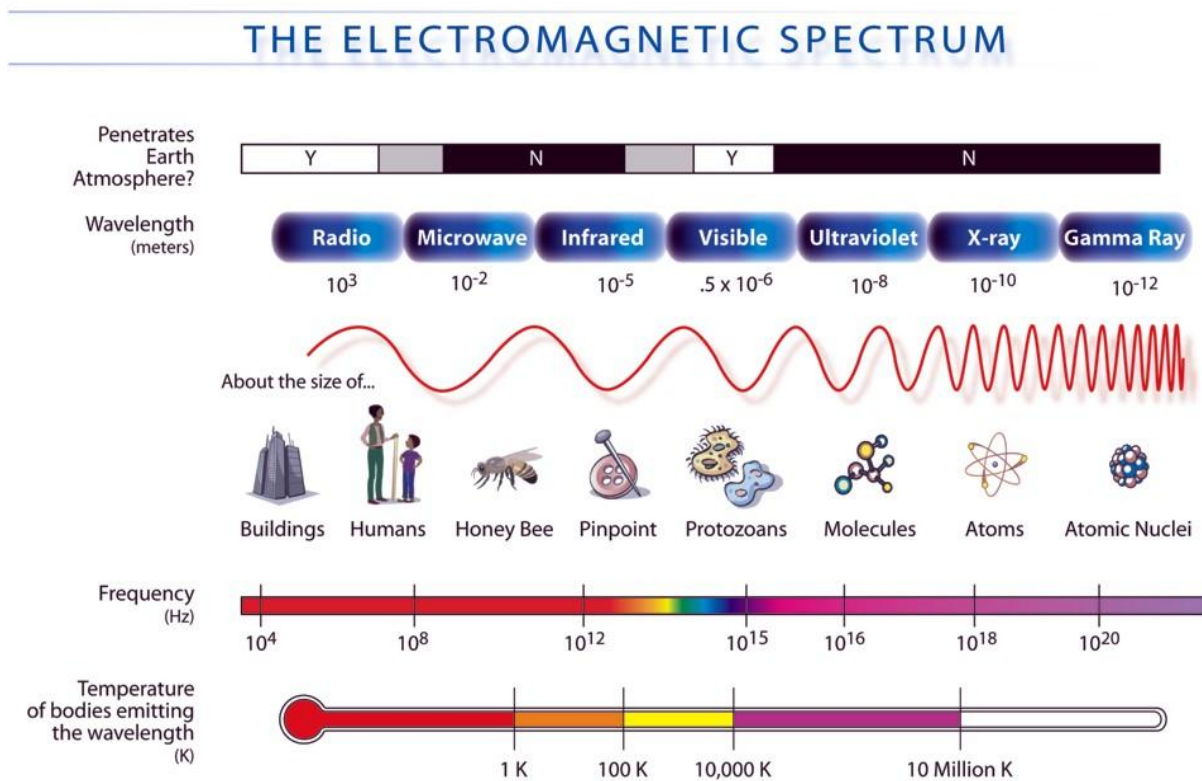
Figure 2b. Electromagnetic spectrum (www.cosmosportal.org).

Figure 3 shows a breakdown of the visible spectrum by frequency and wavelength.

Color	Frequency	Wavelength
violet	668–789 THz	380–450 nm
blue	606–668 THz	450–495 nm
green	526–606 THz	495–570 nm
yellow	508–526 THz	570–590 nm
orange	484–508 THz	590–620 nm
red	400–484 THz	620–750 nm

Figure 3.   Visible spectrum (http://en.wikipedia.org/wiki/Visible_spectrum).

2.2.   Cerenkov Radiation and the Frank-Tamm Theory

A qualitative explanation of Cerenkov emission is gleaned as follows. The polarization phenomenon is illustrated in Fig. 4 (Jelley, 1958), where the circles represent individual atoms. In the absence of the moving charged particle, the atoms are roughly spherical in shape. As the charged particle moves through the medium, its electric field distorts the atoms so that the electrons are displaced to one side and the nuclei to the other thus forming dipoles. The medium becomes polarized about the point P. At relatively low speeds, relative symmetry of the aggregated polarization field surrounds the passing particle so that there is virtually no resultant field at large distances and, therefore, no radiation.
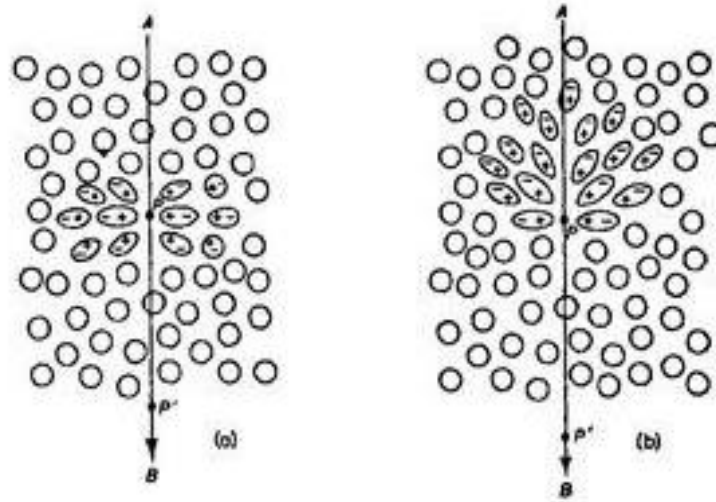
Figure 4.   Polarization inducement by a charged particle moving through matter. Left: relatively slow movement. Right: relatively fast movement (Jelley, 1958, Fig. 1.1).

At relatively high velocities, the polarization field is asymmetric along the path of the particle and extends to some distance from the path. The inducement of this field causes the brief radiation of an electromagnetic pulse. If the velocity of the particle is greater than the phase velocity of the light in the medium, the radiated wavelets can be in phase so that, at a distant point of observation, there is a resultant field. This radiation is only observed at a particular angle θ with respect to the track of the particle. To develop a relationship between the light and the angle, consider Fig. 5.
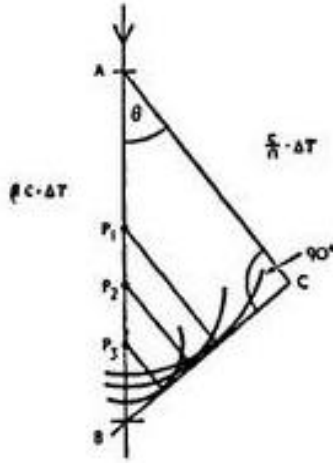
Figure 5.   Huygens construction to illustrate coherence (Jelley, 1958, Fig. 1.2).

If the velocity of the particle is βc, where c is the speed of light in a vacuum, then in a time Δt the particle will move a distance $AB = \beta c \cdot \Delta t$ and the light a distance $AC = \Delta t \cdot (c/n)$, where n is the refractive index of the medium. Then

$$\cos \theta = \frac{1}{\beta n}. \tag{1}$$

The Cerenkov theoretical treatment depicts a charged particle passing through matter in which the nearby electrons are treated as classical oscillators. The electrons are set in motion by the electric field of the passing particle. The field of the charged particle is affected by the polarization of the medium. The Frank-Tamm theory (Frank and Tamm, 1937) was developed using the following simplifying assumptions (Jelly, 1958):

(1) The medium is considered as a continuum so that microscopic structure is ignored. The dielectric constant is the only parameter used to describe the behavior of the medium.

(2) Dispersion is ignored.

(3) Radiation reaction is neglected.

(4) The medium is assumed to be a perfect isotropic dielectric so the conductivity is zero, the magnetic permeability is unity, and there is no radiation absorption.

(5) The particle is assumed to move at constant velocity; i.e., the slowing down due to ionization and the multiple Coulomb scattering are ignored.

(6) The medium is unbounded and the track length infinite.

The byproduct of the development is the Frank-Tamm expression for the energy loss per unit path of a charged particle in a medium as given by

$$\frac{dW}{dl} = \frac{e^2 z^2}{c^2} \int_{\beta n > 1} \left(1 - \frac{1}{\beta^2 n^2} \right) \omega d\omega .$$
(2)

For an electron, the energy loss is of the order of several keV per cm, or ~0.1% of the energy loss by ionization.

Usage of Cerenkov radiation with MCNP6 causes our interest to center on photon emission rather than energy loss. Photon emission can be related to the energy loss expression in Eq.(2) using Plank's quantum equation (Wehr and Richards, 1967),[1]

$$E = h\nu \text{ (MeV/photon)}.$$
(3)

The number of photons N emitted is thus related to the energy loss according to

---

[1] Radiation is emitted in discrete amounts rather than continuously.

$$W = N \cdot h\nu \text{ (MeV)}. \tag{4}$$

The energy emitted per unit path per unit frequency interval is

$$\frac{d^2W}{dld\omega} = \frac{e^2 z^2}{c^2}\left(1 - \frac{1}{\beta^2 n^2}\right)\omega \text{ (MeV/cm-s)} \tag{5}$$

The number of photons emitted per unit path per unit angular frequency interval is

$$\frac{d^2N}{dld\omega} = \frac{e^2 z^2}{\hbar c^2}\left(1 - \frac{1}{\beta^2 n^2}\right). \tag{6}$$

where

$$\hbar = \frac{h}{2\pi}. \tag{7}$$

The frequency ν of the light is related to the angular frequency ω according to

$$\omega = 2\pi\nu \text{ (s}^{-1}). \tag{8}$$

The frequency ν of the light is related to the wavelength λ as

$$\nu = \frac{c}{\lambda} \text{ (s}^{-1}), \tag{9}$$

where c is the speed of light.

The number of photons emitted per unit path per unit frequency interval is

$$\frac{d^2N}{dld\nu} = \frac{d^2N}{dld\omega} \cdot \frac{1}{h\nu} = \frac{4\pi^2 e^2 z^2}{hc^2}\left(1 - \frac{1}{\beta^2 n^2}\right) \text{ (photons/cm-s)}. \tag{10}$$

11

For constant parameters,

$$\frac{dN}{dl} = 2\pi\alpha z^2 \left(\frac{1}{\lambda_2} - \frac{1}{\lambda_1} \right)\left(1 - \frac{1}{\beta^2 n^2} \right) \text{ (photons/cm)}, \qquad (11)$$

where α is the fine structure constant

$$\alpha = \frac{e^2}{\hbar c} = \frac{1}{137.0393} \; . \qquad (12)$$

For piecewise-constant parameters

$$\frac{dN}{dl} = 2\pi\alpha z^2 \sum_{i=1}^{I} \left(\frac{1}{\lambda_i} - \frac{1}{\lambda_{i-1}} \right)\left(1 - \frac{1}{\beta_i^2 n_i^2} \right) \text{ (photons/cm)}. \qquad (13)$$

Integration over the path length given piecewise-constant parameters gives the total photon

emission.

$$N = 2\pi\alpha L z^2 \sum_{i=1}^{I} \left(\frac{1}{\lambda_i} - \frac{1}{\lambda_{i-1}} \right)\left(1 - \frac{1}{\beta_i^2 n_i^2} \right) \text{ (photons)} \qquad (14)$$

Equation (14) forms the basis of the technique used in MCNP6 to do Cerenkov photon emission.

The technique parallels that used for other types of emission, including delayed gamma-rays

(Durkee et al., 2009). Emission is done by first determining the integer number of emitted

photons N_{MCNP6} to be according to

$$N_{MCNP6} = INT(N + rang) \text{ (photons)}, \qquad (15)$$

where INT is the Fortran integer operator and *rang* is the MCNP6 random number function.[2] The value of L is determined by the charged-particle condensed-history routine and is passed to the Cerenkov routine.

Next, the emission wavelength is determined using the cumulative distribution sampling function (CDF). For a constant refractive index, integration of Eq.(10) over length L over wavelength gives

$$\Xi = \frac{N(\lambda)}{N} = \frac{\int_{\lambda_1}^{\lambda} \frac{d^2 N}{dl d\lambda}}{\int_{\lambda_1}^{\lambda_2} \frac{d^2 N}{dl d\lambda}} = \frac{\frac{1}{\lambda} - \frac{1}{\lambda_1}}{\frac{1}{\lambda_2} - \frac{1}{\lambda_1}} = r \quad . \tag{16}$$

where r is a random number between 0 and 1. Eq.(16) can be solved analytically to give the sampled wavelength

$$\lambda = \frac{\lambda_1 \lambda_2}{r(\lambda_1 - \lambda_2) + \lambda_2} \quad . \tag{17}$$

For a piecewise constant refractive index,

$$\Xi_j = \frac{\sum_{i=1}^{j} \left(\frac{1}{\lambda_i} - \frac{1}{\lambda_{i-1}} \right) \left(1 - \frac{1}{\beta_i^2 n_i^2} \right)}{\sum_{i=1}^{I} \left(\frac{1}{\lambda_i} - \frac{1}{\lambda_{i-1}} \right) \left(1 - \frac{1}{\beta_i^2 n_i^2} \right)} = r \quad . \tag{18}$$

which is equated to a random number *r* between 0 and 1. The index j is then determined such that $\Xi_j > rang$ to give the emission band for wavelength λ_j. Sampling of the emission wavelength within the band between $i-1$ and i is then done using another random number[3] so that

---

[2] The rang function generates random numbers between 0 and 1.

$$\lambda = \lambda_{i-1} + r \cdot \left(\lambda_i - \lambda_{i-1} \right) . \tag{19}$$

The time at which Cerenkov photon emission occurs is considered to be instantaneous. Thus, there is no sampling algorithm for emission time.[4]

2.3. Refractive Index Formulations

It is necessary to develop formulations for the refractive index of matter. The theory uses concepts from Maxwell's electrodynamics and atomistic theory. Matter is treated as continuous in Maxwell's theory, yielding a refractive index that is independent of the light wavelength. Experimental observations show that refraction is frequency dependent. An accounting of the atomic structure of matter is required to develop formulations for the refractive index that are wavelength dependent.

An initial formulation for the refractive index is developed by considering the interaction of an electromagnetic wave with matter using classical electrodynamics. Maxwell's equations in a medium are (Born and Wolf, pp. 1–2)

$$
\begin{aligned}
\nabla \times \vec{H} - \frac{1}{c} \frac{\partial \vec{D}}{\partial t} &= \frac{4\pi}{c} \vec{j} \\
\nabla \times \vec{E} + \frac{1}{c} \frac{\partial \vec{B}}{\partial t} &= 0 \\
\nabla \cdot \vec{D} &= 4\pi\rho \\
\nabla \cdot \vec{B} &= 0
\end{aligned}
\qquad , \tag{20}
$$

---

[3] The process parallels that for multigroup delayed-gamma emission (Durkee et al., 2009).

[4] See Durkee et al. 2009 for treatment of finite emission time.

where $\vec{E}$ and $\vec{B}$ are the electric field and magnetic induction vectors, respectively. To describe the effect of the field on matter, the electric current density $\vec{j}$, electric displacement $\vec{D}$, and magnetic vector $\vec{H}$ are used and the electric charge density ρ is introduced. The field vectors $\vec{E}$, $\vec{B}$, $\vec{D}$, $\vec{H}$, and $\vec{j}$ are uniquely determined using supplemental relations to describe the behavior of matter caused by the fields. For time-harmonic fields, matter at rest, and isotropic material, these constitutive relations have the simple form

$$\vec{j} = \sigma \vec{E} \ , \tag{21}$$

$$\vec{D} = \varepsilon \vec{E} \ , \tag{22}$$

and

$$\vec{B} = \mu \vec{H} \ , \tag{23}$$

where σ, ε, and μ are the specific conductivity, dielectric constant, and magnetic permeability. Materials for which σ is small are called insulators or dielectrics. Their electric and magnetic properties are completely determined by ε, and μ. For nonmagnetic substances, μ is close to unity. Materials are termed to be paramagnetic diamagnetic when $\mu > 1$ and $\mu < 1$, respectively.

Optical photon transport can be formulated for nonconducting ($\sigma = 0$) and conducting ($\sigma \neq 0$) media. Media in which light propagates without appreciable weakening (e.g., air, water, glass) are termed transparent. These media are nonconductors — there is little loss of electromagnetic energy and little Joule heat. The following development and the MCNP6 feature treats optical photon transport in nonconducting media.

For a dielectric (non-conducting) medium, application of Maxwell's equations to a plane electromagnetic wave incident on a plane boundary between two homogeneous media yields a

refractive index that is a function of the dielectric constant ε and magnetic permeability μ of the medium (Born and Wolf, pp.10–13)

$$n = \sqrt{\varepsilon\mu} \ .$$

(24)

For many nonmagnetic materials of interest, μ is effectively unity (Born and Wolf, p. 13). Thus, the index of refraction given by Eq. (24) depends on the dielectric constant ε and is independent of the frequency of the electromagnetic wave (Born and Wolf, 1980, p.10–13). Equation (24) is reasonably valid for substances such as gases with a simple chemical structure which does not disperse light substantially; i.e., for substances whose optical properties are relatively invariant with the frequency of light.

The (absolute) refractive index is also measure of the ratio of the speed of an electromagnetic wave in vacuum to that in a medium (Hecht, 1990) as given by

$$n = \frac{c}{v} \ .$$

(25)

Experimental results show that, in general, the refractive index is frequency dependent. This constitutes the phenomenon of dispersion (Born and Wolf, 1980, p. 90). The dependence of the dielectric parameter ε and the index of refraction n is treated by taking into account the atomic structure of matter (Born and Wolf, 1980, p 13). Electromagnetic field theory itself is inadequate in treating emission, absorption, and dispersion of light.

The interaction of an electromagnetic field with matter can be done using a simple model. The vectors $\bar{B}$ and $\bar{D}$ are expressed as the sum of two terms, the first treating the vacuum field

16

and the second arising from the influence of matter. Two new vectors describe the effects of matter: the electric polarization $\vec{P}$ and the magnetic polarization $\vec{M}$. Thus, instead of using Eqs.(22) and (23), we have

$$\vec{D} = \vec{E} + 4\pi\vec{P} \ . \tag{26}$$

and

$$\vec{B} = \vec{H} + 4\pi\vec{M} \ . \tag{27}$$

These expressions portray the production of polarization $\vec{P}$ and $\vec{M}$ in a volume element by the electromagnetic field (see Fig. 4) that is, to first order, proportional to the field. Each volume element contains a source of a secondary or scattered wavelet. The total field is comprised of the incident field and the combination of all secondary wavelets.

In the atomic theory the interaction of particles (atoms and molecules) are modeled. These particles produce a field which varies inside the matter. This internal field is modified by any externally applied field. The properties of the matter are derived by averaging over the total field within the matter. If the region over which the averaging is done is large compared to the linear dimensions of the particles, the electromagnetic properties of each can be simply described by an electric and a magnetic dipole. The secondary field is then the field caused by these dipoles. In this approximation it is assumed that $\vec{P}$ and $\vec{M}$ are proportional to $\vec{E}$ and $\vec{H}$ so that

$$\vec{P} = \eta\vec{E} \ . \tag{28}$$

and

17

$$\vec{M} = \chi \vec{H} \ . \tag{29}$$

Using Eqs.(22), (23), (28), and (29) we see that

$$\varepsilon = 1 + 4\pi\eta \ . \tag{30}$$

and

$$\mu = 1 + 4\pi\chi \ . \tag{31}$$

Thus, atomistic theory can be formulated such that the matter is regarded as made of molecules which are polarizable so that under the influence of an external field they exhibit electric and magnetic moments. As an approximation, it may be assumed that the components of these moments are linear function of the field components. The formulations are dependent on the nature of the matter. Here we confine our attention to isotropic, non-magnetic substances.

The total field $\vec{E}$ acting on a molecule is comprised of (1) the mean field $\bar{\bar{E}}$ in a region surrounding the molecule and containing many molecules, and (2) the field inside of the region surrounding the molecule caused by several molecules surrounding the central molecule. It can be shown that (Born and Wolf, pp. 85–86)

$$\vec{E} = \bar{\bar{E}} + \frac{4\pi}{3} \vec{P} \ . \tag{32}$$

The assumption is made that, for each molecule, the electric dipole moment $\vec{p}$ caused by the electric field is proportional to the field so that

$$\vec{p} = \alpha_p \vec{E} \ , \tag{33}$$

where α_p is the mean polarizability. The total polarization due to all N molecules is

$$\vec{P} = N\vec{p} = N\alpha_p \vec{E} \ .$$ (34)

Eliminating $\vec{E}$ from Eqs.(32) and (33) with (34), the dielectric susceptibility η is

$$\eta = \frac{N\alpha_p}{1 - \frac{4\pi}{3}N\alpha_p} \ .$$ (35)

Substituting this into Eq.(30) gives

$$\varepsilon = \frac{1 + \frac{8\pi}{3}N\alpha_p}{1 - \frac{4\pi}{3}N\alpha_p} \ .$$ (36)

Using Maxwell's relation between the dielectric parameter ε and the index of refraction n as given in Eq.(24) for a dielectric medium ($\mu = 1$), Eq.(36) can be rewritten as

$$\alpha_p = \frac{3}{4\pi N}\frac{\varepsilon - 1}{\varepsilon + 2} = \frac{3}{4\pi N}\frac{n^2 - 1}{n^2 + 2} \ ,$$ (37)

which is known as the Lorentz-Lorenz formula. This expression connects Maxwell's theory with the atomistic theory of matter, providing a link between the mean polarizability α_p and the index of refraction n.

Given the link between Maxwell's field theory and the atomistic theory provided in Eqs.(26)–(37), a simplified model of the dispersion of light in a nonconducting medium can be modeled as

19

follows (Born and Wolf, pp. 91–97). First, the displacement $\vec{r}$ of each electron in the medium from its equilibrium position is found. The displacement is characterized using the Lorentz force law

$$\vec{F} = Q\left(\vec{E} + \frac{\vec{v}}{c} \times \vec{B}\right) , \tag{38}$$

where Q is the charge of the electron. The electron behaves, to a good approximation, as an oscillator with respect to its equilibrium position according to the quasi-elastic restoring force

$$\vec{F}_e = -q_r \vec{r} , \tag{39}$$

where q_r is the restoring-force constant. Letting m denote the mass of the electron, its equation of motion is

$$m\ddot{\vec{r}} + q_r\vec{r} = Q\vec{E} . \tag{40}$$

Denoting ω to be the angular frequency of the incident field,

$$\vec{E} = E_0 e^{-i\omega t} , \tag{41}$$

and taking

$$\vec{r} = \vec{r}_0 e^{-i\omega t} , \tag{42}$$

then

$$\vec{r} = \frac{Q\vec{E}}{m\left(\omega_0^2 - \omega^2\right)} , \tag{43}$$

where

20

$$\omega_0 \sqrt{\frac{q}{m}} \qquad (44)$$

is the resonance (or absorption) frequency. According to Eq.(43) the electron oscillates with the frequency of the incident field.

Each electron contributes to the polarization a moment (neglecting the contributions from the nuclei)

$$\vec{p} = Q\vec{r} \; . \qquad (45)$$

Using Eqs.(34), (43), and (45), the total polarization is

$$\vec{P} = N\frac{e^2}{m}\frac{\vec{E}}{\left(\omega_0^2 - \omega^2\right)} \; . \qquad (46)$$

Using Eqs.(34) and (46),

$$N\alpha_p = N\frac{e^2}{m}\frac{1}{\left(\omega_0^2 - \omega^2\right)} \; . \qquad (47)$$

Substituting Eq.(47) into Eq.(37) gives

$$\frac{n^2 - 1}{n^2 + 2} = \frac{4\pi}{3}\frac{Ne^2}{m\left(\omega_0^2 - \omega^2\right)} \; , \qquad (48)$$

21

which is the expression for the frequency dependent refractive index.

Equation (48) is problematic when $\omega = \omega_0$. The matter is resolved by including a damping contribution to the equation of motion to represent energy dissipation (due to collisions between the atoms). With the damping force, equation of motion becomes

$$m\ddot{\vec{r}} + g\dot{\vec{r}} + q\vec{r} = Q\vec{E} \ , \tag{49}$$

so that the displacement is

$$\vec{r} = \frac{Q\vec{E}}{m\left(\omega_0^2 - \omega^2\right) - i\omega g} \ . \tag{50}$$

The polarization is thus a complex quantity.

Matter actually has many resonant frequencies. Thus, Eq.(48) generalizes to

$$\frac{4\pi}{3}N\alpha = \frac{n^2 - 1}{n^2 + 2} = \frac{4\pi}{3}N\frac{e^2}{m}\sum\frac{f_k}{\left(\omega_k^2 - \omega^2\right)} \ , \tag{51}$$

where Nf_k is the number of electrons corresponding to the resonance frequency ω_k.

For gases $n \sim 1$, so that Eq.(51) can be simplified to

$$n^2 - 1 = 4\pi N\alpha = \sum_k \frac{\rho_k}{\left(v_k^2 - v^2\right)} = \sum_k \frac{\rho_k}{c^2}\frac{\lambda^2 \lambda_k^2}{\left(\lambda^2 - \lambda_k^2\right)} \ , \tag{52}$$

where

22

$$\rho_k = N\frac{e^2}{\pi m}f_k \ , \tag{53}$$

and

$$v_k = \frac{\omega_k}{2\pi} = \frac{c}{\lambda_k} \ . \tag{54}$$

Following the application of mathematical identities and series expansions for Eq.(52), the Cauchy form for the wavelength-dependent refractive index for a dielectric (non-conducting) medium

$$n(\lambda) = A + \frac{B}{\lambda^2} + \frac{C}{\lambda^4} + \frac{D}{\lambda^6} \tag{55}$$

is obtained. The validity of Eq.(55) is predicated on the assumption that $n \sim 1$, which is the case for gases.

For substances of high density, i.e. liquids or solids, it is not permissible to replace n by unity in the denominator of term two in Eq.(51). In this case, it can be shown that the expression

$$n(\lambda) = \left(1 + \frac{B_1\lambda^2}{\lambda^2 - C_1} + \frac{B_2\lambda^2}{\lambda^2 - C_2} + \frac{B_3\lambda^2}{\lambda^2 - C_3} \right)^{1/2} \ , \tag{56}$$

is obtained. This frequency-dependent expression for the refractive index is known as the Sellmeier dispersion formula (Born and Wolf, 1980, p. 97).

More complicated formulations that include temperature and pressure dependence are found in the literature (Schiebener et al., 1990), but these are not currently supported in MCNP6.

2.4.   MCNP6 Cerenkov Feature

The MCNP6 Cerenkov feature can be executed using analog or nonanalog photon creation. Because large numbers of Cerenkov photons can be created by each charged particle, it is advisable to use biased creation. Biasing will limit the number of photons created, while preserving tally data.

The refractive index can be calculated using three formulations. These formulations are appropriate for optical photon transport in nonconducting media:

(1) A constant, frequency-independent refractive index.

(2) The four-term Cauchy formula can be used to calculate the frequency-dependent refractive index. This is most suitable for gases.

(3) The three-term Sellmeier frequency-dependent refractive index. This is most suitable for liquids and solids. (Born and Wolf, 1980, pp. 93–97).

3. VERIFICATION SIMULATIONS

We are interested in demonstrating that the MCNP6 Cerenkov emission functions correctly. This interest includes a demonstration that emission as a function of wavelength is treated properly.

Verification simulations have been executed to confirm that the MCNP6 Cerenkov emission executes as desired. Perl script **cr.pl** was written to calculate Cerenkov photon emission given piecewise constant parameters prescribed by Eq.(14). For direct comparison of the MCNP6 and **cr.pl** results, a write statement was implemented in MCNP6 subroutine emit_cerenkov to provide the termwise photon yields for Eq.(14). MCNP6 and **cr.pl** calculations were executed for (1) each term in the series and (2) the total number of emitted photons. This treatment ignores photon transport in the medium which can be done by MCNP6 but is not done by **cr.pl**.

MCNP6 does Cerenkov emission for each source charged-particle in a history. Each source particle is emitted at the stipulated source energy. Condensed history treatment is done to transport each charged particle. The algorithm determines a step size, which is passed to the Cerenkov subroutine for use as the value L in Eq.(14). For the verification simulations, a write statement was used to provide this value for the initial step in the condensed history transport of the source particle. This value was then used in **cr.pl** to calculate the total photon emission.

The test problems include (1) 4-MeV electrons in water and (2) 4000-MeV alphas in water.

The MCNP6 calculations were executed using an Intel serial build on the Pete cluster. The directory is: `/home/jdurkee/old_pete/MCNP6_CRNKV`.

3.1. Test 1: 4-MeV Electrons in Water

The MCNP6 model consists of a point source of 4-MeV electrons in a sphere 2 mm in diameter. Photon production is calculated by the emission formula in Eq.(14). The refractive

25

index is calculated using the Cauchy and Sellmeier expressions given in Eqs.(55) and (56), respectively. Data for the Cauchy coefficients are A = 1.3199, B = 6.878e-2, C = 1.132e-3, D = 1.14e-4 (Kohl et al., 1995).[5] The Sellmeier coefficients are B_1 = 5.6840-e-1, C_1 = 5.1018e-3, B_2 = 1.7262e-1, C_2 = 1.8211e-2, B_3 = 2.0862e-2, C_3 = 2.6207e-2 (Daimon and Masumra, 2007).[6] In addition, a calculation is executed using the first term in the Cauchy formulation for the refractive index, 1.3199 ("constant" calculation).

The MCNP6 refractive-index calculations were executed using file inpcr. The calculations were executed with a serial Intel build on the Pete cluster. One history was executed. Print triggers were placed in subroutine **emit_cerenkov.F90** to provide the calculated refractive index data.

MCNP6 calculated the value L = 5.7432e-2 cm for the first condensed-history step for a 4-MeV electron in water. This value is used in **cr.pl** for the analytic refractive-index calculations.

Figure 6 shows plots of the index of refraction of water at 20C using the Cauchy and Sellmeier expressions and coefficient calculated using MCNP6 and **cr.pl**. Appreciable difference in the refractive index for the two formulations is apparent. According to the theory, the Cauchy expression is appropriate for gases, while the Sellmeier expression is more suitable for liquids (Born and Wolf, 1980, pp. 93–97). We simply report this observation – it does impact the photon

---

[5] The cited research used the Cauchy expression to characterize the refractive index for water. Given the theoretical development in Eqs.(52)–(56), the use of the Cauchy formulation may not be valid. We do not debate validity here, but simply note the issue and apply the formulation.

[6] Daimon and Masumura provide coefficients for a four-term expansion. We use terms 1–3 in our testing using their data for 20 C in accordance with Eq.(56).

production. According to the literature, the wavelength-independent refractive index for water is 1.33 (Jelley, 1958, p. 24). Thus, the Cauchy data appear to be high.
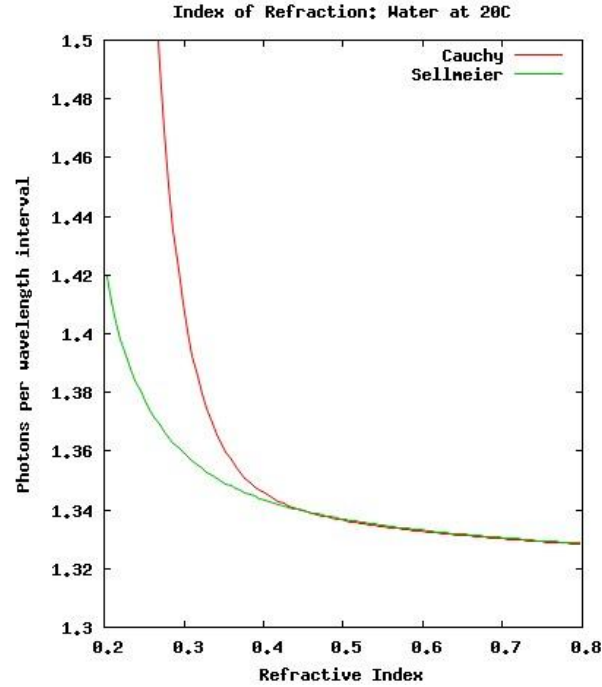

Figure 6. Cauchy and Sellmeier refractive index in water at 20C. MCNP6 and **cr.pl** results overlay to within resolution.

Figure 7 shows the results calculated using MCNP6 and **cr.pl** for the termwise evaluation of Eq.(14) and the Cauchy and Sellmeier refractive index formulations in Eqs.(55) and (56). The MCNP6 and **cr.pl** results are identical for the Cauchy and Sellmeier formulations. The emission for the Cauchy and Sellmeier formulations is in good agreement above 0.35 μm. At shorter wavelengths, the predictions diverge – likely due to the Cauchy and Sellmeier coefficients and/or regimes of applicability.
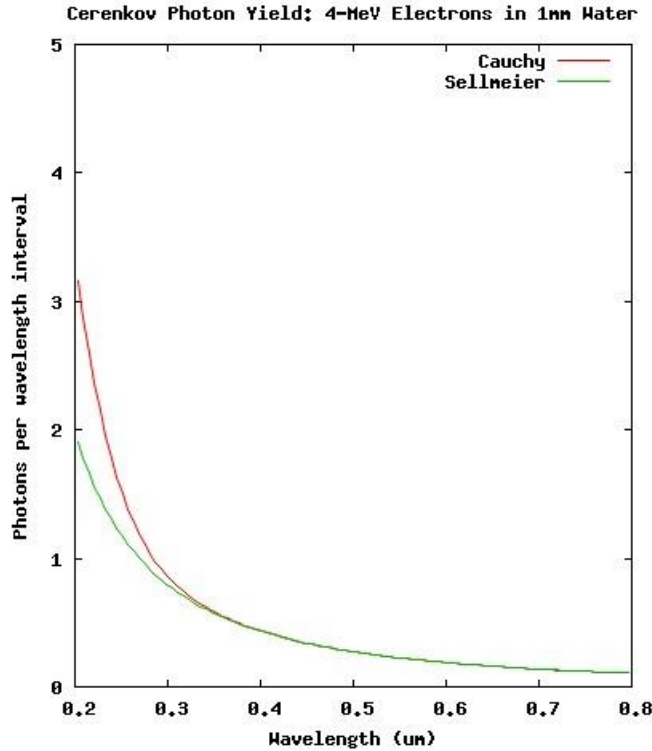
Figure 7. Cerenkov emission spectrum for 4-MeV electrons in water calculated using MCNP6 (patched) and **cr.pl**. Identical results are obtained using both codes.

The total number of emitted photons calculated using the three refractive-index formulations are listed in Table 1. All results are dentical for MCNP6 and **cr.pl**. The predictions for the Cauchy refractive index are almost 30% greater than that for the constant refractive index. The prediction made using the Sellmeier data are within 10% of the prediction made using the constant refractive index.

Table 1. Total Cerenkov emission for 4-MeV electrons in 5.7432e-2 cm water calculated using Eq.(14)

Refractive Index Formulation	Total Cerenkov Photon Emission
Constant	41.5
Cauchy	53.1
Sellmeier	45.1

The MCNP6 surface-integrated "F1" tally was used to register the number of optical photons crossing the surface of the water sphere. This tally calculates the number of photons in an energy bin. Comparison against the optical-photon source, shown in Fig. 6, requires conversion of the tally to wavelength bin. The relation is given using Planck's relation in Eq.(3) and the relationship between the wavelength and frequency of light given in Eq.(9). Thus,

$$\lambda = \frac{hc}{E} \ (\mu m). \tag{57}$$

The conversion of an energy bin to a wavelength bin is

$$E_i - E_{i-1} = h(v_i - v_{i-1}) = hc\left(\frac{1}{\lambda_i} - \frac{1}{\lambda_{i-1}}\right) = hc\left(\frac{\lambda_{i-1} - \lambda_i}{\lambda_i \lambda_{i-1}}\right)(\text{MeV}). \tag{58}$$

The number of particles contributing to a tally $F1_\#$ in an energy bin is related to the number of particles crossing a surface by

$$F1_E = F1_\# \cdot \left(E_i - E_{i-1}\right)(\text{photons}). \tag{59}$$

Using Eqs.(58) and (59), the number of particles contributing to a tally in a wavelength bin is

$$F1_\lambda = F1_\# hc\left(\frac{\lambda_{i-1} - \lambda_i}{\lambda_i \lambda_{i-1}}\right)(\text{photons}). \tag{60}$$

The number of photons in an energy bin is thus equal to the number in a wavelength bin.

The MCNP6 optical photon emission calculations were also executed using inpcr. The calculations were executed with a serial Intel build on the Pete cluster (with deactivated print triggers for the refractive index in subroutine **emit_cerenkov.F90**). The F1 tally data were calculated using 200 bins between 1 eV and 1 keV and 20 bins between 1 keV and 1 MeV. The

29

calculations were executed using 1000 and 10000 source electron histories. Execution using the constant, Cauchy, and Sellmeier expressions with 1000 source histories required 0.47, 0.30, and 0.27 minutes, respectively, while execution using 10000 histories required 2.9, 3.7, and 3.2 minutes, respectively. Relative uncertainties in the F1 tallies for most of the optical spectrum (0.2 to 0.8 μm or 6.208e-6 to 1.552e-6 MeV) were less than 0.05 using 1000 histories and less than 0.01 using 10000 histories.

Equation (60) was implemented in **cr.pl** to calculate wavelength-dependent emission using the MCNP6 energy-dependent F1 tally data.[7]   The results are shown plotted in Fig.8. The tally binning causes the slight piecewise structure. The results for 1000 histories give a non-smooth structure to the emission profiles. Execution using 10000 source electrons improves the results. The underlying structure suggests a bluish/violet color at the surface of the water per Fig. 3. Here again applicability of the Cauchy expression is to gases may be causing the exaggerated emission at short wavelengths versus the Sellmeier and constant refractive indices (Born and Wolf, 1980, pp. 93–97).

---

[7] The MCNP6 F1 energy-dependent tally data were placed in files F11CE and F11SE for input and use by **cr.pl** to produce wavelength-dependent data for plotting.
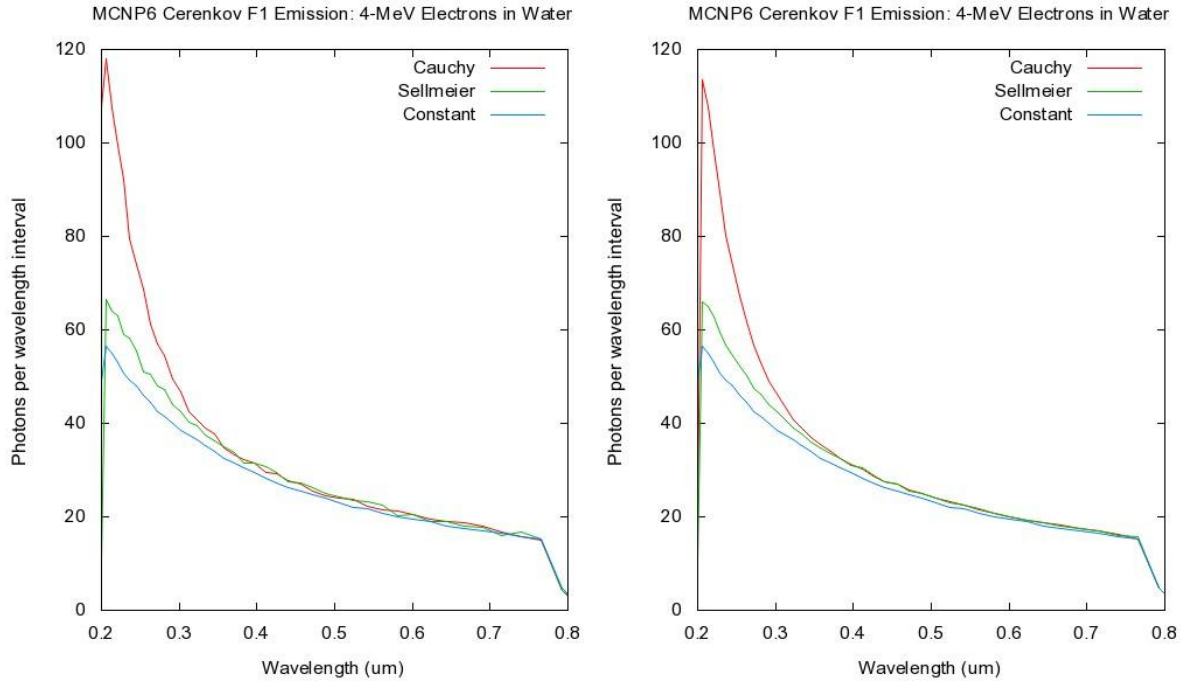
Figure 8. Cerenkov emission spectrum at the surface of the water for 4-MeV electrons in water calculated using MCNP6 (patched). NPS = 1000 (left) and 10000 (right).

The Cerenkov emission in Fig. 8 shows a steep drop at approximately 0.76 μm. This emission behavior was investigated two ways. First, Figure 9 shows the CDFs for 4-MeV electrons in water as calculated using the Cauchy and Sellmeier formulations. The CDFs are well behaved.
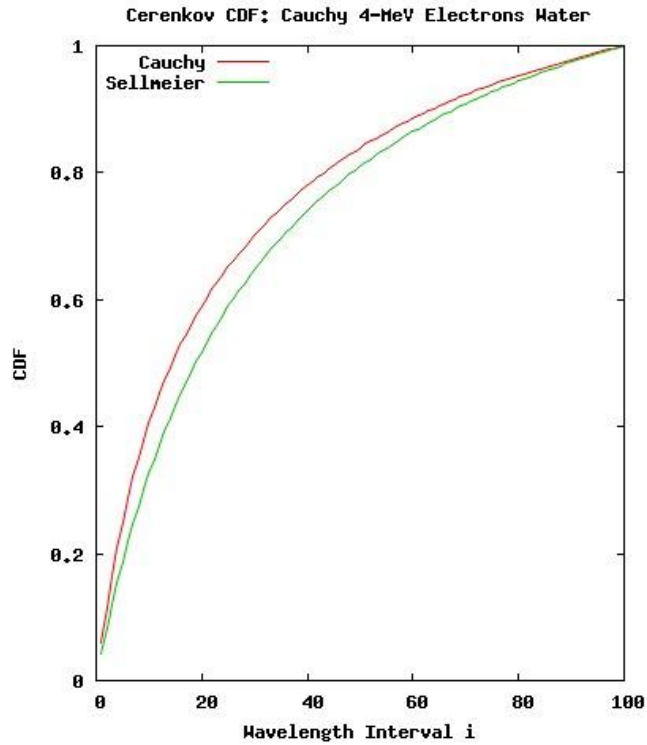
Figure 9. CDFs for 4-MeV electrons in water calculated using Cauchy and Sellmeier formulations.

Second, an additional array, cpsave, was added to subroutine emit_cerenkov.F90 for debugging studies. As the wavelength for each optical photon was sampled during a calculation, cpsave was incremented (by one) and the energy bin recorded. At the end of the calculation, the array contents were printed. Those data are plotted in Fig. 10. As is apparent, there is no abrupt drop in the higher wavelength bins. Something is thus impacting the F1 tallies, Fig. 8.
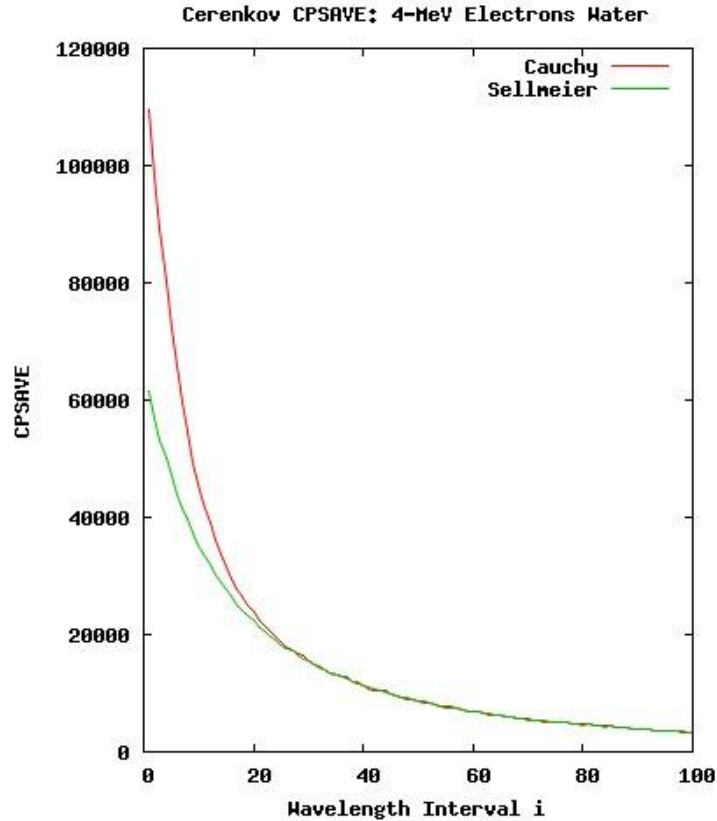
32

Figure 10. Sampled photon emission in subroutine emit_cerenkov.F90 for 4-MeV electrons in water calculated using Cauchy and Sellmeier formulations.

Execution was tested using analog and biased Cerenkov photon creation. The bias factor ckvnum was set to 0.1, meaning that 10% of the photons created using analog execution were created. Execution time for 2000 source electrons for analog and biased execution required 3.4 m and 1.9 m, respectively. Results were the same for analog and biased simulations.

3.2. Test 2: 4000-MeV alphas in Water

The MCNP6 model consists of a point source of 4000-MeV alphas a sphere 50 cm in diameter. Photon production is by the emission formula in Eq.(14). The refractive index is

33

calculated using the Cauchy and Sellmeier expressions given in Eqs.(55) and (56), respectively, using the data in Section 3.2. In addition, a calculation is executed using the first term in the Cauchy formulation for the refractive index, 1.3199 ("constant" calculation).

The test file is inpcra. The F11 photon-tally calculations were executed with a serial Intel build on the Pete cluster using 1000 source histories. Execution using the Cauchy, Sellmeier, and constant expressions required 1.73, 0.60, and 0.48 minutes, respectively. Relative uncertainties in the F1 tallies were on the order of 0.03 or less for each calculation.

MCNP6 execution required the use of phys:a 4000 to set EMAX = 4000. This permits MCNP6 to treat energies above the normal maximum energy. MCNP6 calculates the value $L =$ 2.1675 cm for the first condensed-history step for a 4000-MeV alpha in water. This value was used in **cr.pl** for the analytical calculations.

Figure 11 shows the results calculated using MCNP6 and **cr.pl** for the termwise evaluation of Eq.(14) with the Cauchy and Sellmeier refractive index formulations in Eqs.(55) and (56). The MCNP6 and **cr.pl** results are identical for the Cauchy and Sellmeier formulations. The emission for the Cauchy and Sellmeier formulations is in good agreement above 0.35 μm. At shorter wavelengths, the predictions diverge – perhaps due to the experimental Cauchy and Sellmeier coefficients and/or regimes of applicability (discussion associated with Eqs.(52)–(56)).
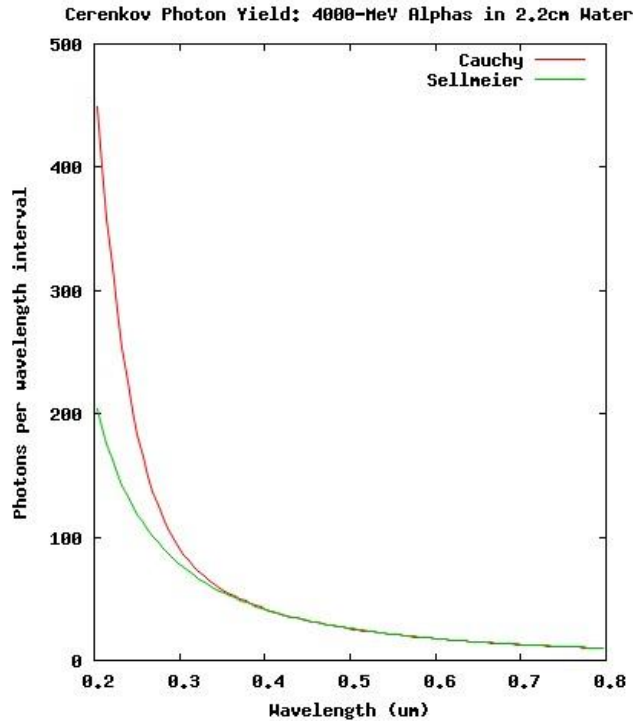
Figure 11. Cerenkov emission spectrum for 4000-MeV alphas in water calculated using MCNP6 (patched) and **cr.pl**. Identical results are obtained using both codes.

The total number of emitted photons calculated using the three refractive-index formulations are listed in Table 2. All results are identical for MCNP6 and **cr.pl**. The predictions for the Cauchy refractive index are almost 30% greater than that for the constant refractive index. The prediction made using the Sellmeier data are within 10% of the prediction made using the constant refractive index.

Table 2. Total Cerenkov emission for 4000-MeV alphas in 2.1675 cm water calculated using Eq.(14)

Refractive Index Formulation	Total Cerenkov Photon Emission
Constant	3755.6
Cauchy	5982.9
Sellmeier	4424.0

35

The MCNP6 Equation (60) was used to calculate wavelength-dependent emission using the MCNP6 F1 tally data. The MCNP6 F1 tally was calculated using logarithmic 200 bins between 1 eV and 1 keV, and 20 bins between 1 keV and 1 MeV. The results are shown in Fig. 12. It is interesting to note that 1000 histories provided results that were converged so as to give smoothly varying and visually appealing results. The underlying structure suggests a bluish/violet color at the surface of the water per Fig. 3.
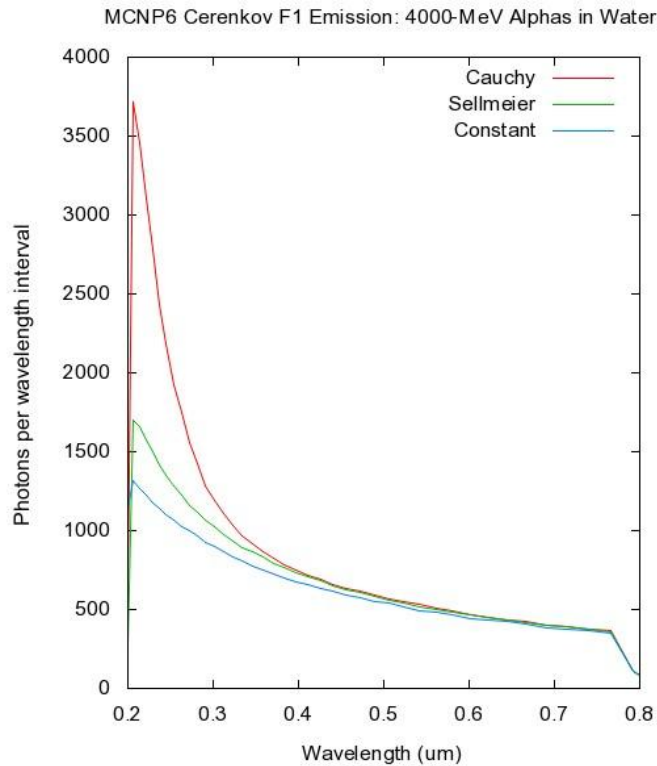

Figure 12. Cerenkov emission spectrum at the surface of the water for 4000-MeV alphas in water calculated using MCNP6 (patched).

Figure 13 shows the CDFs for 4000-MeV alphas in water as calculated using the Cauchy and Sellmeier formulations. The CDFs are well behaved, but differ somewhat from the CDFs for 4-MeV electrons in water.
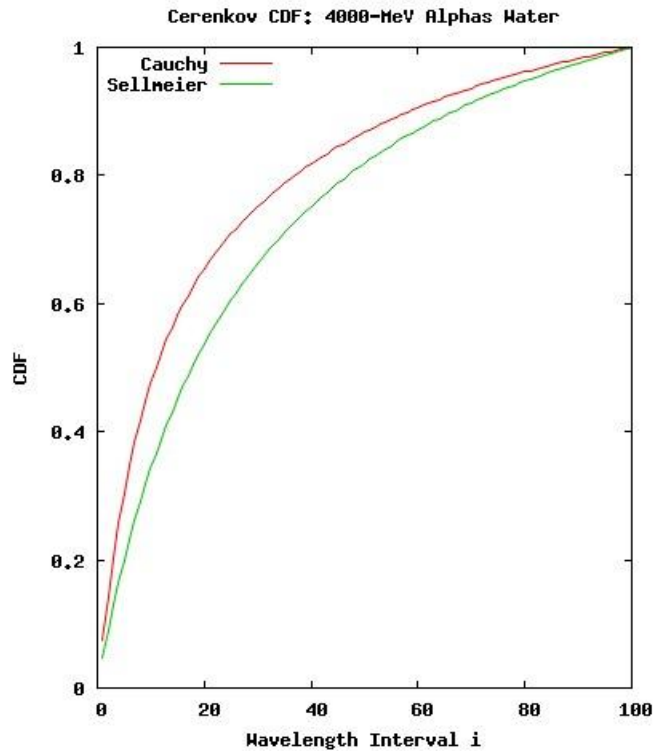
36

Figure 13. CDFs for 4000-MeV alphas in water calculated using Cauchy and Sellmeier
formulations.

The cpsave data for are plotted in Fig. 14. As is apparent, there is no abrupt drop in the higher

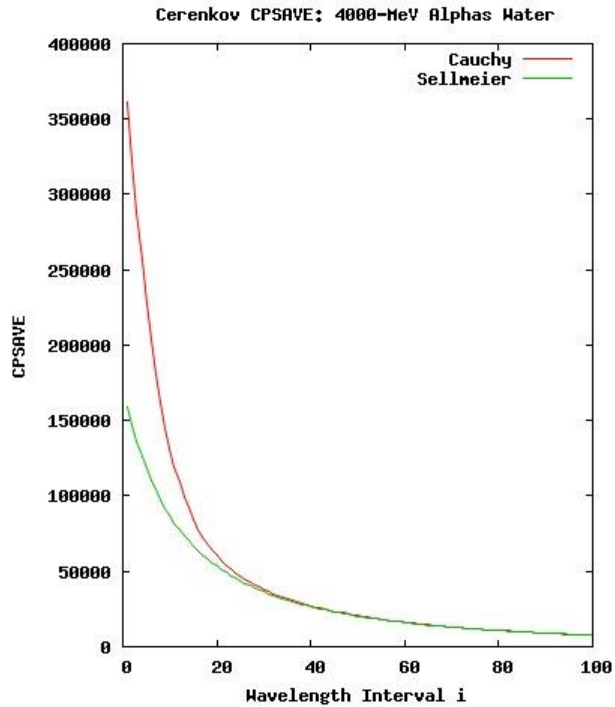wavelength bins. Something is thus impacting the F1 tallies, Fig. 12.

Figure 14. Sampled photon emission in subroutine emit_cerenkov.F90 for 4-MeV electrons in water calculated using Cauchy and Sellmeier formulations.

Execution was tested using analog and biased Cerenkov photon creation. The MCNP6 input file bias factor ckvnum was set to 0.1, meaning that 10% of the photons created using analog execution were created.

4. VALIDATION SIMULATIONS

Simulations validating the results against experiments were not performed. No satisfactory validation data could be found.

5. SUMMARY AND CONCLUSIONS

The Los Alamos MCNP6 code has been upgraded to treat Cerenkov photon emission. The feature includes three options for the refractive index calculation: (1) constant (wavelength invariant), (2) the Cauchy form, which is appropriate for gases, and (3) the Sellmeier expression, which is suitable for liquids and solids.

In support of this feature, verification calculations have been executed for models of (1) 4-MeV electrons in water and (2) 4000-MeV alpha particles in water. The results show that the emission spectra for Cerenkov radiation are executed correctly by MCNP6 for a serial Intel executable. The F1 tally for optical photon emission at the surface of the water may show questionable behavior. MPI parallel execution gives F1 tallies results are in close agreement with their serial counterparts for electron and alpha models using constant, Cauchy and Sellmeier refractive indices.

REFERENCES

Born M. and Wolf E., 1980. *Principles of Optics*, Pergamon Press, New York, p. 90.

Cerenkov P.A., 1934. "Coherent Visible Radiation of Fast Electrons Passing Through Matter," *Dokl. Akad. Nauk SSSR* 14, 107–112.

Daimon M. and Masumura A., 2007. "Measurement of the Refractive Index of Distilled Water from the Near-Infrared Region to the Ultraviolet Region," *Applied Optics*, **46 (18)**, 3811–3820.

Durkee, J.W. Jr., James M.R., McKinney G.W., Trellue H.R., Waters L.S., and Wilson W.B., 2009. "Delayed-Gamma Signature Calculation for Neutron-Induced Fission and Activation Using MCNPX, Part I: Theory," *Progress in Nuclear Energy*, **51**, 813–827.

Fermi E., 1940. "The Ionization Los of Energy in Gasses and in Condensed Materials," *Physical Review* 14, 485–493.

Frank I. and Tamm Ig., 1937. "Coherent Visible Radiation of Fast Electrons Passing Through Matter," *Dokl. Akad. Nauk SSSR* **14**, 107–112.

Goorley, T., James, M., Booth, T., Brown, F., Bull, J., Cox, L.J., Durkee, J., Elson, J., Fensin, M., Forster, R.A., Hendricks, J., Hughes, H.G., Johns, R., Kiedrowski, B., Martz, R., Mashnik,

S., McKinney, G., Pelowitz, D., Prael, R., Sweezy, J., Waters, L., Wilcox, T., and Zukaitis, T., 2012. "Initial MCNP6 Release Overview," *J. Nuclear Technology*, **180**, 298–315.

Hecht E., 1990. *Optics*, Addison-Wesley Publishing Company, Reading, Massachussetts, p. 56.

Hughes H.G., 2012. "Recent Developments in Low-Energy Electron/Photon Transport for MCNP6," Los Alamos National Laboratory report LA-UR-12-24213.

Jelley J.V., 1958. *Cerenkov Radiation and Its Applications*, Pergamon Press, New York, p. 1–31.

Kohl, M., Essenpreis, M., and Cope M., 1995. "The Influence of Glucose Concentration Upon the Transport of Light in Tissue-Simulating Phantoms," *Physics in Medicine and Biology,* **40**, 1267–1287.

Schiebener P., Straub J., Sengers J.M.H., and Gallagher J.S., 1990. "Refractive Index of Water and Steam as a Function of Wavelength, Temperature, and," *J. Phys. Chem. Ref. Data,* **19 (3)**, 677–717.

Wehr. M.R. and Richards J.A., 1967. *Physics of the Atom*, Addison-Wesley Publishing Company, Reading, Massachussetts, p. 76.